Features of Power Quality in Single-Phase Distributed Power Generation Using Adaptive Nature Vectorial Filter

Ashutosh K. Giri, Amin Qureshi, Sabha Raj Arya, *Senior Member, IEEE*, Rakesh Maurya, *Member, IEEE*, and B. Chitti Babu, *Senior Member, IEEE*

***Abstract*—This paper presents the new controller for voltage and frequency control (VFC) of two-winding single-phase induction generator. It provides coordinated control of battery energy storage system (BESS) and dump load during the mismatch of power between loads and generator using VFC loop. It provides protection against overcharging of BESS. For this purpose adaptive vectorial filter (AVF) is implemented to operate single-phase induction generator in standalone mode of operation for power quality features. The unique feature of this filtering technique is its simplicity and no other analogy filters are required to produce the reconstructed signal of fundamental frequency. This procedure uses the vectorial natures of the single-phase input signal, which is decomposed by shifting property in the α–β orientation frame in order to get the diverse harmonic constituents. The design and analysis of AVFs for the proposed system is carried out in order to find the required performance. The proposed control method is evaluated by simulations in MATLAB/Simulink followed by experimental validation in laboratory for signifying its capability to execute different harmonic constituents under an extremely distorted generator current. Apart from control method, design of generator with finite-element method and its electromagnetic properties are also discussed.**

***Index Terms*—Adaptive vectorial filter (AVF), battery energy storage system (BESS), finite-element method (FEM), frequency locked loop (FLL), voltage regulation, voltage source converter (VSC), wind power.**

I. Introduction

THE nonconventional energy sources, such as wind, solar, biomass, and hydro, are looking as a trustworthy options to the conventional energy sources such as fossil fuel [1]. The main reason behind shifting our focus from fossil fuel to natural resources is due to depletion level of coal, petroleum, and gas. As per estimates coal reserve would be critically low after 130 years and oil availability would be critical after 40 years [2]. Therefore, the new millennium belongs to sustainable energy sources. Due to increasing level of pollution and green house emission, the world is gradually looking for green and clean energy [3]. In sustainable energy growth, the solar and wind energy based generations experience a huge growth worldwide [4]. In last two decades due to development of semiconductor devices and its control, the standalone asynchronous generators have been the first choice among all available peer generators for tapping the energy from the wind velocity and mini/microhydro energy due to its less maintenance, low cost, and robust structure [4]. The main problem with induction generator is its voltage and frequency variation under variable loads (linear and nonlinear). Hence, in this paper, more attention is given over controlled performance of generator with the help of custom power device such as DSTATCOM. The control strategy of said device decides the overall performance of the generator. In the available literatures, ample number of techniques based on transformation, time domain, and frequency domain (adaptive as well as nonadaptive) are reported [4]–[23]. Blaabjerg *et al.* [5] presented an outline of the structures for the distributed power generation system (DPGS) based on fuel cell, solar photovoltaic, and wind turbines. Apart from this, control techniques of the grid-side converter are presented, and the prospect of mitigation for low-order harmonics is also discussed. Singh *et al.* [6] have given the idea of battery-based voltage and frequency controller for parallel operation of isolated asynchronous generators. Some battery constraints, such as size and regular maintenance, are still remains unaddressed. Rajgopal *et al.* [7] have used the instantaneous reactive power theory (IRPT) for controlling the DSTATCOM operated in shunt with the load in DPGS. This theory is nonadaptive in nature, therefore, filter coefficient cannot be adjusted to get modified reference source current. Further, IRPT fails to produce desired fundamental component in variable frequency supply. Rao *et al.* [8] has explored the instantaneous symmetrical component theory for load compensation under unbalance supply voltage conditions. In [9], the modified PQ theory based algorithms are presented. PQ theory is not able to address the distorted supply waveform. To eliminate the problem in said theory, Huang and Wu [9] have added a three-phase sinusoidal waveform generator that is capable of generating the desired waveform. The research paper [10] presents various nonactive power filtering techniques in time domain. Fair comparison has also made. In three-phase four-wire system, three techniques namely IRPT (PQ Theory), the synchronous reference frame theory, and peak detection method are compared and studied. The technical as-

Manuscript received November 7, 2017; accepted December 22, 2017. Date of publication January 3, 2018; date of current version August 7, 2018. Recommended for publication by Associate Editor M. Liserre Gae. *(Corresponding author: Sabha Raj Arya.)*

A. K. Giri, A. Qureshi, S. R. Arya, and R. Maurya are with the Department of Electrical Engineering, Sardar Vallabhbhai National Institute of Technology, Surat 395007, India (e-mail: ashu_ee2002@rediffmail.com; amin4047@gmail.com; sabharaj1@gmail.com; rmaurya@eed.svnit.ac.in).

B. C. Babu is with the Department of Electrical Engineering, University of Nottingham, Semenyih 43500, Malaysia (e-mail: chittibabu.b@nottingham.edu.my).

Color versions of one or more of the figures in this paper are available online at http://ieeexplore.ieee.org.

Digital Object Identifier 10.1109/TPEL.2017.2789209

sessment is done by taking into account the robustness for the operation with unstable and deformed supply voltages, uneven load currents, control signals conditioning, etc. [11]. An adaptive antialiasing filter for three-phase application is presented in detail [12]. This filter attenuates interharmonics as well as lower order harmonics from the supply current under distorted load current. At the same time due to presence of buffers in intermediate stages, the delay in the signal transformation is the main problem. In [13], electronic load controller is presented for voltage and frequency control of the self-excited induction generator (SEIG). This controller is working in constant power mode without any energy storage elements. The performance of DSTATCOM is extensively implemented for power quality improvement in three-phase system using leaky LMS algorithms by Arya and Singh [14]. It had operated in zero voltage regulation mode and power factor correction mode. In [7]–[14], the voltage and frequency control is achieved by using either dc link or BESS connected at the terminal of dc link. In the most of the literatures, excess of power generated by the generator has been dumped or stored in the BESS but the provision of charging control of BESS is untouched. In this paper, authors have tried to review literature in two areas: 1) the work already done in the area of distributed generation for improving the power quality, and 2) various control strategies available for operating the voltage source converter (VSC) for voltage and frequency control. The papers [1]–[14] and [15]–[29] belong to the area of power quality and control techniques, respectively. Sinnak [15] proposed a method for directly and strongly estimating the phase, frequency, and amplitude of variable frequency single-phase signals for such applications, which is a phase-locked loop (PLL) method based on a structure. Guo *et al*. [16] presented a multiple-complex coefficient-filter-based PLL. Its unique quality lies in the precise and speedy extraction of the positive and negative sequence components from the polluted grid voltage. Arabloue *et al.* [17] have suggested the gradient-descent total least-squares (GD-TLS) algorithm. The local convergence of the GD-TLS algorithm is studied and bounds for its step-size that make sure its stability. This paper [18] presents the topology description of injection type hybrid active power filter (IHAPF) and recognizes an electrical model. To advance the presentation of IHAPF, generalized integral proportional–integral (PI) control is projected. The control method is usually useful and appropriate to erstwhile active filters. Bhattacharya *et al.* [19] have proposed different kind of shunt compensation scheme. Suresh *et al*. [20] have proposed fuzzy logic based controller for active filtering. In [21], a novel circuit configuration for the three-phase shunt active power filter (APF) is proposed to contain harmonic currents. This is prepared with a two-leg bridge converter, an interfacing inductor, compensating capacitors, and a high-frequency noise filter capacitor/resistor. This paper [22] surveyed the foremost results in iterative learning control investigation. Trouble in stability, performance, learning fleeting manners, and robustness were discussed along with four design techniques that have emerged as among the most accepted. In [23], the finite-element analysis is presented. With the help of this analysis, electromagnetic behavior of machine is presented under different operating conditions. In [24], the battery energy storage system (BESS) based wind energy system is discussed for frequency control. Battery charging and discharging is shown under various loading conditions. In the literature [25]–[28], some advanced control techniques based on neural networks and fuzzy logic controllers are also used. The important characteristic of these techniques are that they do not require the exact mathematical design of the system because they are based on fuzzy principal and not on crisp philosophy. But the real challenge of any fuzzy logic based controller is its hardware realization. In [29], an adaptive type vectorial filter is used for reconstructing the fundamental signal of 50 Hz from the distorted input signal. The widespread use of low-pass filters on the distorted currents or another based on transformed is also a widely used technique. However, the new concept in adaptive vectorial filter (AVF) is that the used filter works on the principle of a PLL which is estimating the magnitude of the vector that is being filtered. Therefore, it has no delay from the input, and gives a very fast responds on spontaneous changes, such as wind velocity. Hence, authors have chosen this filter to implement for the improvement in the power quality of the proposed system. In comparison with preceding complex coefficient filters used for extraction of positive- and negative-sequence harmonic components [16], the vectorial property approach has been followed to get the final complex coefficient of AVF of the single-phase input signal in the α–β reference frame. In this way, the proposed scheme is different from the earlier approaches because vectorial nature of the input signals provides valuable features for the amendment of the design constants. The benefit of the method is that these constants can be selected to offer a required and predefined performance. Additionally, this method can be realized on hardware with DSP without much trouble at low computational cost.

In this paper, a new control topology incorporating BESS and dump resistor is employed to control the SEIG operation with AVF [29]. The main advantage of coordinated control of BESS and dump resistor is protection against overcharging of battery and hence life of battery will increase. The dump controller acts only when battery is charged to the specified voltage level during light load conditions. The AVF approach is used to mitigate harmonics in the supply current of single-phase induction generator feeding linear/nonlinear load running with wind turbine. Additionally, the reactive power compensation is achieved using the same algorithm. AVF is very special in the sense of its exceptional characteristic lies in the precise and hasty extraction of the α–β components from the contaminated grid voltage. Moreover, harmonic components can also be computed precisely, which has the latent use for discriminatory compensation in APF applications. This technique decomposes bivariate functions in empirical mode. It is not based on extrema but only on some distinguishing points correlated to a definite convexity. The substance of this method is that it does not use the shifting procedures. It provides the theoretical expression of the decomposition, which avoids the drawbacks of shifting. Besides this, it is also able to decompose exactly the signal into elementary intrinsic modes function and take apart quickly revolving and oscillating components.

II. System Configuration

The configuration of the proposed DPGS is shown in Fig. 1. A single-phase two-winding SEIG rotated by the wind turbine is feeding power to linear and nonlinear load. For nominal voltage generation, one shunt capacitor is used in auxiliary winding, which supports self-excitation of the SEIG at the time of starting. This capacitor is required for supplying reactive power to

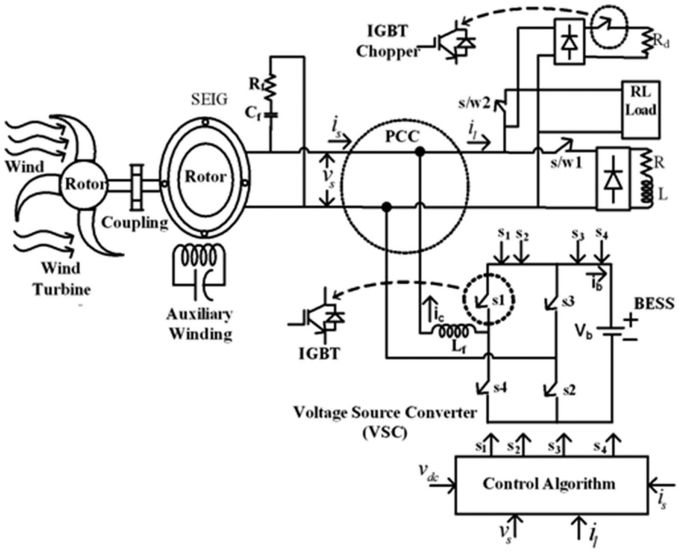

Fig. 1. Schematic diagram of proposed system.

generate nominal voltage at no load. A DSTATCOM with BESS is connected in shunt at the load end for harmonic and reactive power compensation in the load current. The DSTATCOM consists of an interfacing inductor (Lf) and two legs of insulated gate bipolar transistors (IGBTs). For minimizing the high-frequency noise in the compensating current, an interfacing inductor (Lf) is connected between VSC and point of common coupling (PCC).

To filter out high-frequency switching noise of VSC, a single unit of first-order-damped high-pass filter (R_f, C_f) is connected at the PCC. The nonlinear load consists of universal diode bridge rectifier along with resistance and inductance. Apart from nonlinear load, one linear and dump load is also connected in the proposed system. The dump load is turn on to control the frequency when battery is charged to the specified safe level that is the excess power generated is diverted toward dump load. Usually, the compensating current generated from VSC-based DSTATCOM supply the reactive power and harmonics of the load current so that distortion in the source current due to nonlinear loading on the generator is reduced to the distortion level as per IEEE standards-519-2014.The switches rating used in VSC is dependent on the amount of reactive power and harmonic current to be compensated. The rest of the design parameter values are given in Appendixes A and B.

III. Design Consideration

The system under consideration includes wind turbine and SEIG as foremost components. However, selected value of excitation capacitor is also very significant part because it not only influences the voltage build-up process with no load but also affect frequency and electromagnetic torque as well. Each component is designed as per system requirement. Its design is given in following sections.

A. Design of Wind Turbine [1]

The selection of proper wind turbine rating is extremely important, which is working as a prime mover for a generator. The available mechanical power for energy conversion is dependent on power coefficient (c_p), wind velocity (v_w), and area of the blade (a). The actual mechanical power output can be written as

$$p = \frac{1}{2} c_p(\eta, \beta) \pi r^2 v_w^3 \tag{1}$$

where r, v_w, β are the radius of blade (m), wind speed (m/s), and the air density (kg/ m^3), respectively. The performance coefficient varies with the wind speed, angular speed of generator, angle of attack, and pitch angle. In general, c_p is dependent on tip speed ratio, and blade pitch angle, θ (deg). The definition of tip speed ratio (η) is given under

$$\eta = \frac{\omega_R r}{v_W} \tag{2}$$

where ω_R is the angular velocity in radian per second. The angular velocity (ω_R) is found by the following relation:

$$\omega_R = \frac{2\pi n}{60}. \tag{3}$$

Power rating of the generator: 2238 W and efficiency is 80% [2]. Mechanical input required at generator: $2238/.80 = 2797$ W, assuming 5% mechanical loss [3] in gear boxes, etc., turbine output $\text{power} = 2797 + 2797 \times 5/100 = 2936$ W.

From (1), radius of swept area (r) can be obtained with known values of $c_P(\eta, \theta)$, β, and v_w. Here, these are taken as 0.48, 1.12, and 12 m/s, respectively, and the value of r is calculated and found to be 1.41 m.

B. Design of Induction Generator

Numerical techniques such as finite-element method (FEM) [24] enable us to work out no load and full load magnetic fields in the various parts of induction generator. Electromagnetic field analysis using FEM has been a subject of careful research in the past two decades [24]. The foremost benefit of the FEM is listed as follows:

1) the exact modeling of the generator's flux circuit, magnetic nonlinearity, material nonhomogeneity, and the effect of discrete winding layouts can be accounted;
2) the idea about voltage and current waveform can be generated by looking flux pattern in the core by this analysis;
3) the analysis completely includes the effects of time and space harmonics at no load and full load;
4) its potential to accord with both steady-state and transient machine operations, without using simplifications, such as those made in conventional machine theory. The field solutions offer machine performance directly, without using the equivalent circuit parameters.

In this section, the FEM design of a single-phase two-winding induction generator is presented in detail for guessing the performance of SEIG in standalone mode of operation. The few result obtained from FEM analysis are presented in Table I for the machine taken into consideration. From Table I, it is clear that flux linkage and total MMF of the selected magnetic path is below the permissible limits prescribed in [24] for the selected machine. The investigation from this method is shown in Fig. 2(a)–(c). In Fig. 2(c), contour mesh and finite elements are presented. For making method more accurate, large no of finite elements have been taken. There are 36 208 nodes and 72 222 elements in it. Current density plot is given in Fig. 2(a) by the color code. Colors of light greens are given in the bottom of the plot. The same color is reflected in the machine cross section. This means that in entire section of the machine winding the cur-

TABLE I
PERFORMANCE OF GENERATOR USING FEM ANALYSIS

Sr. No.	Particulars	Values
1.	2-D planar (depth)	76 cm
2.	No. of nodes	36 208
3.	No. of elements	72 222
4.	Total current in the circuit	5 A
5.	Voltage drop	16 V
6.	Flux linkage	0.0104452 Wb
7.	Flux/current	0.00208904 H
8.	MMF drop along contour	0.334693 Amp-turns
9.	Average H.t	1.20237

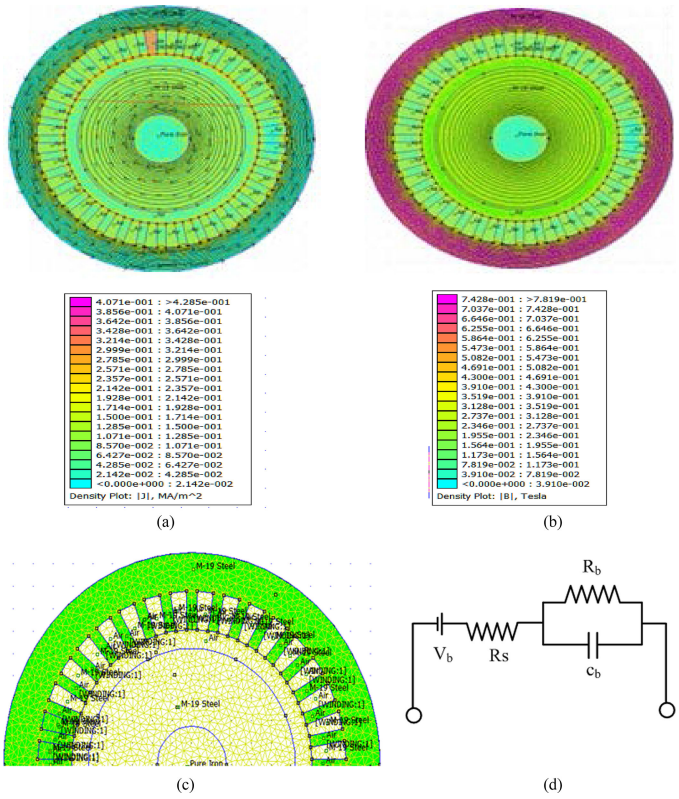

Fig. 2. Finite-element analysis of induction generator. (a) Flux orientation for stator and rotor parts and color code current density plot [J]. (b) Flux density plot with color code (c) created mesh and elements for half-section of machine. (d) BESS Circuit model.

rent density is uniform. It is seen that flux lines are distributed uniformly in the stator and rotor when current is flowing from windings in the stator and rotor.

In addition to this, the flux density plot is also obtained in the form of color code in Fig. 2(b). For 5-A current in the stator winding, 0.0104452 Wb of flux is created in the core of four-pole machine. It clearly shows that flux is distributed uniformly along the pole cross section. The flux density is presented in stator and rotor windings in Fig. 2(b), where its color code is indicating about safe zone of operation.

C. Design of BESS

BESS Thevenin's equivalent circuit model is used for its dynamic and static characteristic study. The parameters of BESS such as V_b represents the open-circuit voltage of battery, R_s refers heat loss element of battery, which is due to electrodes resistance, connectors, and separator. The parallel branch of R_b and C_b depicts the effect of over voltage during polarization reaction process. For design purpose battery is considered to have 2.2 kW, 6 h of peak capacity, and 34 batteries, 12 V each. Positive voltage regulation is considered 10% from no load to full load.

Then, from energy balance equation polarizing capacitor can be calculated as follows:

$$0.5\, C_b V_b^2 = \text{Total kWh}$$
$$C_b = 2.2 \times 6 \times 3600 \times 10^3 / 0.5\left(400^2 - 350^2\right)$$
$$= 2534 \text{ F}.$$

Generally, the value of R_b is taken in the range of 5–10 kΩ for making longer (in hours) charging and discharging time for the better life of the battery. The value of R_s is taken very less to keep losses as minimum as possible. Generally, R_s is taken between 0.5 and 0.1 Ω.

IV. CONTROL STRATEGY

A block diagram of the AVF-based control algorithm is shown in Fig. 3(a). Single-phase reference source current is derived using fundamental active and reactive power component of sensed load current. The reactive power needed to SEIG and consumer is supplied by the VSC to maintain the constant terminal voltage (nominal value).The voltage at PCC (v_s), load current (i_L), and source current (i_s) are used as input signals for this algorithm. The basic elements of the control algorithm used for computation of active and oscillating constituents of reference source current and total reference source current for generation of gating signal are shown in Fig. 3(a). The details of AVF are being discussed in length as follows.

A. Model of AVF Filter

This section presents structure of the AVF filter. For understanding the principal of AVF in voltage and frequency control application of the SEIG, let us assume a vector quantity $i_{l\alpha\beta}$, i.e., two components of a distorted load current as an input taken in the α–β reference frame, which is stationary in nature.

This input is represented as follows:

$$i_{l\alpha\beta} = A_P \begin{Bmatrix} \cos\ \omega t \\ \sin\ \omega t \end{Bmatrix}. \tag{4}$$

Here, one assumption is that the parameter ω is changing very slightly or almost constant. This can be considered a valid assumption because in standalone-based distributed generation system, large variation cannot be allowed. Hence, the subsequent investigation is an accurate estimate for this purpose. Therefore, it is likely to compute the derivative over the time of $i_{l\alpha\beta}$ as

$$\frac{di_{l\alpha\beta}}{dt} = \omega M i_{l\alpha\beta}. \tag{5}$$

Here, matrix M is expressed as

$$M = \begin{pmatrix} 0 & -1 \\ 1 & 0 \end{pmatrix}. \tag{6}$$

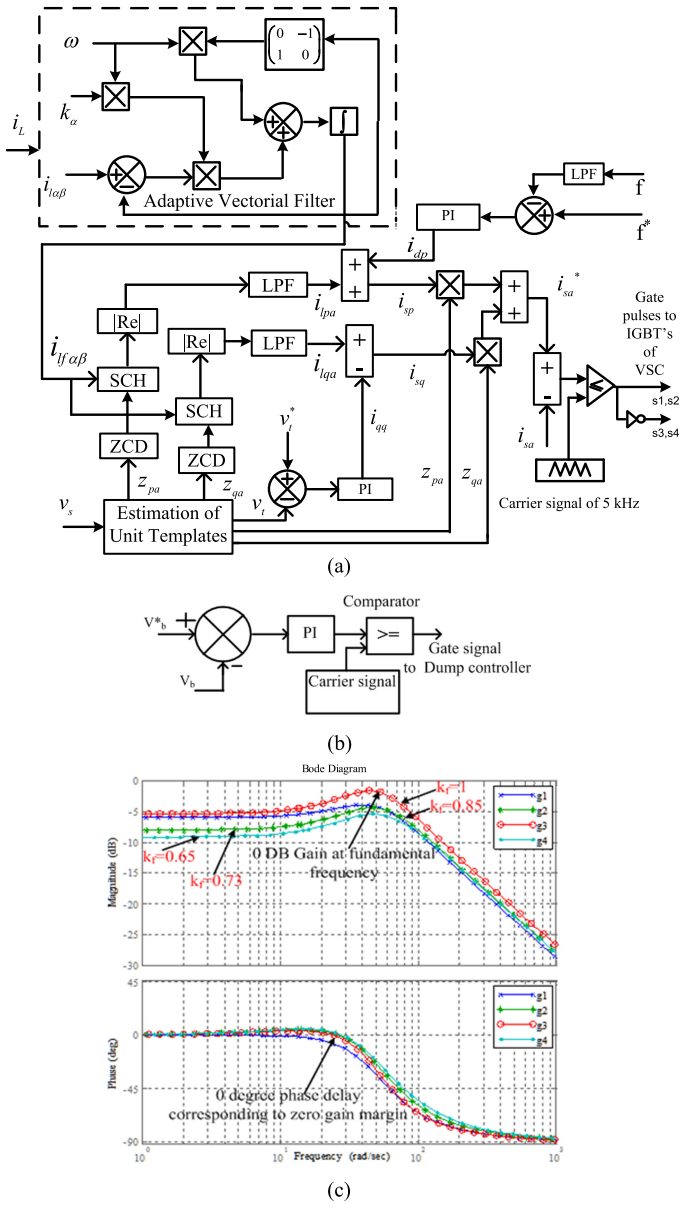

Fig. 3. (a) Block diagram of AVF control algorithms. (b) Bode plot of AVF for $\omega = 50$ Hz and different value of k_f. (c) Bode plot of AVF for $\omega = 50$ Hz and different value of k_f.

Let $i_{lf\alpha\beta}$ be fundamental component of load current and treated as the output vector of the AVF filter. Now, the scalar and vectorial products of $i_{l\alpha\beta}$ and $i_{lf\alpha\beta}$ are written as

$$w_p = i_{lf\alpha\beta}^T i_{l\alpha\beta} \tag{7}$$

$$x_p = i_{lf\alpha\beta}^T M i_{l\alpha\beta}. \tag{8}$$

The change in w_p and x_p with respect to time can be calculated from the following equations:

$$\frac{dw_p}{dt} = \left(\frac{d}{dt} i_{lf\alpha\beta}^T + w i_{lf\alpha\beta}^T M\right) i_{l\alpha\beta} \tag{9}$$

$$\frac{dx_p}{dt} = \left(\frac{d}{dt} i_{lf\alpha\beta}^T + w i_{lf\alpha\beta}^T M\right) M i_{l\alpha\beta}. \tag{10}$$

Here, the intention is to recreate $i_{l\alpha\beta}$ from $i_{lf\alpha\beta}$, then, it have to be fulfilled that

$$w_p \to w_p^* = i_{l\alpha\beta}^T i_{l\alpha\beta} \tag{11}$$

$$x_p \to x_p^* = 0. \tag{12}$$

With the help of (11) and (12), (9) and (10) can be extended to identify the expression of $i_{lf\alpha\beta}$ in such a way that it gets these objectives.

If ϖ is defined as

$$\varpi \triangleq w_p - w_p^* \tag{13}$$

Therefore, (9) can be changed into

$$\frac{d\varpi_p}{dt} + k_{wp}\varpi_p + \frac{dw_p^*}{dt} - k_{wp}\varpi_p = \left(\frac{di_{lf\alpha\beta}^T}{dt} + \omega i_{lf\alpha\beta}^T M\right) i_{l\alpha\beta}. \tag{14}$$

From (14), it is encountered that selecting

$$\frac{dw_p^*}{dt} - k_{sp}\varpi_p \triangleq \left(\frac{di_{lf\alpha\beta}^T}{dt} + \omega i_{lf\alpha\beta}^T M\right) i_{l\alpha\beta}. \tag{15}$$

Hence

$$\frac{d\varpi_p}{dt} + k_{sp}\varpi_p = 0. \tag{16}$$

It is concluded that (15) indicating about a linear system with first order and ϖ_p tends exponentially toward zero when $k_{wp} > 0$. Therefore, clause given in (14) is satisfied. Equation (15) can be simplified regarding (7) and that *sp* is a constant. In that case, (15) is rewritten as

$$k_{sp} i_{l\alpha\beta}^T i_{l\alpha\beta} = \left(\frac{di_{lf\alpha\beta}^T}{dt} + \omega i_{lf\alpha\beta}^T M + k_{sp} i_{lf\alpha\beta}^T\right) i_{l\alpha\beta}. \tag{17}$$

Therefore, the dynamical expression $i_{lf\alpha\beta}$ must fulfill as given

$$\frac{d}{dt} i_{lf\alpha\beta}^T + \omega i_{lf\alpha\beta}^T M + k_{sp} i_{lf\alpha\beta}^T = k_{sp} i_{l\alpha\beta}^T + k_1 i_{l\alpha\beta}^T M. \tag{18}$$

On the similar lines from (10), the dynamics of $i_{lf\alpha\beta}$ must be defined as

$$\frac{d}{dt} i_{lf\alpha\beta}^T + \omega i_{lf\alpha\beta}^T M + k_{xp} i_{lf\alpha\beta}^T = k_2 i_{l\alpha\beta}^T. \tag{19}$$

It is observed that conditions (11) and (12) ought to be fulfilled concurrently. For attaining this, coefficients k_{sp}, k_1, k_{xp}, and k_2 must be taken properly. Here, the coefficients are taken as follows:

$$k_{sp} = k_{xp} = k_2 = \omega k_f$$

$$k_1 = 0.$$

In these circumstances, (18) and (19) go ahead to the similar formulation as

$$\frac{di_{lf\alpha\beta}}{dt} = \omega M i_{lf\alpha\beta} + \omega k_f (i_{l\alpha\beta} - i_{lf\alpha\beta}). \tag{20}$$

Equation (20) represents the dynamic of $i_{lf\alpha\beta}$. It is seen that (20) is used to recreate an input signal having frequency ω. In this manner, if ω is taken as a strange constraint that can be estimated in true time, then (20) would be made adaptive.

The assessment of the output signal can be estimated using the control block diagram shown in Fig. 3(a) that has been articulated in its vectorial form.

B. Computation of Active and Reactive Unit Voltage Template and In-Phase Component of Reference Source Current

The SEIG terminal voltage can be computed as follows:

$$v_t = \sqrt{V_p^2 + V_q^2}. \tag{21}$$

Here, V_p and V_q are the components in-phase and quadrature of PCC voltage of induction generator. The component of PCC voltage, which is in quadrature, can be generated using phase-shifting block. The PCC voltage may be presented as

$$V_p = v_t \ \sin \ \omega t \tag{22}$$

$$V_q = v_t \ \sin(\omega t - \pi/2). \tag{23}$$

Here, v_t and ω are the instantaneous supply voltage and angular frequency at the PCC of SEIG, respectively. The load current (i_L) may be expressed in terms of in phase current component (i_{fp}), quadrature current component (i_{fq}) and harmonic current (i_h) as

$$i_L = i_{fp} + i_{fq} + i_h. \tag{24}$$

The both unit templates of PCC voltage are derived as follows:

$$z_{pa} = \frac{V_P}{v_t} \tag{25}$$

$$z_{qa} = \frac{V_q}{v_t}. \tag{26}$$

An AVF-based control [29] in the α–β reference frame with selected frequency and band of frequency is used to derive the fundamental component of load current ($i_{lf\alpha\beta}$) as shown in Fig. 3(a). In this computation process, the difference of fundamental component of load current and sensed load current in vector form is taken for estimating the error signal. This error signal is multiplied with frequency adaptation coefficient $k_f \ \omega$ and subsequently added with the derivative over the time of vectorial fundamental load current. Thereafter by taking integration, the load fundamental component in vector form is obtained. The important feature of this algorithm is that low-pass filter is not used in the core part of computation. Thus, it is simple and fast in dynamical system. For recreation of fundamental load component in vector form, the value of k_f can be selected for a definite settling time T_s. For example, if 0.01 is tolerance factor for fundamental component, then $k_f \approx 4.6/(\omega T_s)$. Furthermore, T_s will be taken relative to the number of periods of the input signal that ought to be used to restructure the signal. Again, if factor *k* is preferred as the number of periods with *k* > 0, then $T_s = kT_0$. Ultimately considering that $\omega = 2\pi/T_0$, the design coefficient can be computed as $k_f \approx 0.73k$. If sampling frequency is taken to 10 kHz, and the number of periods to rebuild the input signal is selected to be $k = 1$; thus, the value of k_f is finally 0.73. Now α and β components are produced at the input of sample and hold logic circuit separately by demultiplexing the α–β components for the generation of reference current. With the help of unit templates and zero-crossing detectors (ZCD), triggering pulses are created to operate the sample and hold (SCH) circuit. The sample and hold logic circuit gives complex valued signal, therefore, the real component of the SCH output gives the amplitude of fundamental active power components (i_{lpa}). First-order low-pass filters are used to separate the low-frequency components. To get the in-phase component of the reference source current, (i_{lpa}) is added with current component of power (i_{dp}), which is required to maintain frequency at constant level. Current component (i_{dp}) of power to maintain the loss in VSC can be obtained as follows.

The error generated in the frequency control loop of VSC at *i*th sampling moment is given as

$$f_e\,(i) = f^*\,(i) - f\,(i)\,. \tag{27}$$

Here, $f^*(i)$ is the reference frequency and *f*(*i*) is the sensed frequency of terminal voltage. The output of the PI controller employed in frequency control loop of VSC at *i*th sampling instant is estimated as

$$i_{dp}\,(i) = i_{dp}\,(i-1) + k_{dp}\,\{f_e\,(i) - f_e\,(i-1)\} + k_{di} f\,(i)\,. \tag{28}$$

Here, $i_{dp}(i)$ represents the power loss, k_{dp} and k_{di} are the PI gain constants of the PI controller.

The active power current components amplitude of the reference source current i_{sp} is calculated as $i_{sp} = i_{dp} + i_{lpa}$ and reference in-phase component of source current is as per the expression given as

$$I_{sp}^* = i_{sp} z_{pa}\,. \tag{29}$$

C. Computation of Reactive Component of Reference Source Current

In order to sustain constant terminal voltage at the PCC, oscillating component of reference source currents is required for the reactive power compensation through DSTATCOM. On the similar lines as per Section IV-B, the reactive power component of the fundamental load current (i_{lqa}) is obtained. The ZCD generate trigger pulses for sample and hold logic (SCH) on which the fundamental load current has been applied as an input signal. The sample and hold logic circuit gives complex signal, therefore, it is required to separate out real and reactive components. The reactive component of the SCH output is considered as amplitude of fundamental reactive power components of load current. First-order low-pass filter is used to extract its smooth or ripple-free component. The voltage error (v_{te}) of a PCC voltage at the *i*th sampling instant is given as

$$v_{te}\,(i) = v_t^*\,(i) - v_t\,(i)\,. \tag{30}$$

This error is tuned for minimum value through PI controller. The output of PI controller (i_{qq}) at the *i*th sampling instant is given as follows:

$$i_{qq}\,(i) = i_{qq}\,(i-1) + k_{pt}\,\{v_{te}\,(i) - v_{te}\,(i-1)\} + k_{it} v_{te}\,(i)\,. \tag{31}$$

Here, $i_{qq}(i)$ is a part of the oscillating power constituent of source current and it is named as (i_{qq}). k_{pt} and k_{it} are the proportional and integral gain constants of the PCC voltage PI controller. The amplitude of reactive power current components of the reference source current (i_{sq}) is computed by $i_{sq} = i_{qq} - i_{lqa}$ and reference quadrature component of source current is as per

$$I_{sq}^* = i_{sq} z_{qa}\,. \tag{32}$$

D. Computation of Reference Source Current and Generation of Gate Pulses

The reference source current is computed by addition of active component of reference source current and reactive component of reference source current as

$$I_s^* = I_{sp}^* + I_{sq}^*. \tag{33}$$

The source current (I_s) sensed and this computed reference source current (I_s^*) are compared and obtained current error is amplified using PI controller. Now, current error signal and carrier signal of 5 kHz are fed to the input of comparator for the generation of gating signals for switching the IGBTs.

E. Frequency Control of SEIG

The frequency of SEIG is maintained constant by satisfying the power balance equation as $P_{\text{gen}=} P_{\text{cons}} \pm P_{\text{battery}} + P_{\text{dump}}$; where P_{gen} is the output generated by the SEIG, P_{cons} is the power feed to consumer load, P_{battery} is battery power, and P_{dump} is the power supplied to the extra load known as dump resistor. For frequency control either actual frequency or power generated by the SEIG can be engaged as a feedback signal. Due to uncertainty in the input power of generator, frequency is a more suitable variable for feedback and hence taken in the planned system. If power is taken as a feedback variable, it may create the problem of tuning in the frequency control loop due to seasonal changes in mechanical input. The dump load circuit comprising a resistor connected in series with an IGBT chopper switch. The operation of dump controller depends on the battery level voltage. Unless and until battery does not attain its optimal charging level dump controller will be inactive. When battery is near to attain its maximum safe voltage level, dump controller diverts excess generated power toward dump resistor for frequency control. Thus, BESS and dump controller working in coordination for frequency as well as battery charging control.

F. Charging Control of BESS

The characteristics of charging/discharging of the BESS are the matter of essential SOC constraints. The characteristic equations of the BESS are given [25] as follows:

$$p_b(k) = x_{dch}(k)p_{dch}(k) - x_{ch}(k)p_{ch}(k) \tag{34}$$

$$x_{ch}(k) \in \{0,1\}, x_{dch}(k) \in \{0,1\} \tag{35}$$

$$soc(k+1) = (1-\alpha)soc(k) + (x_{ch}p_{ch}(k)\mu_{ch} - x_{dch}p_{dch}(k)/\mu_{dch})\Delta k/v_b \tag{36}$$

where the charging power is represented by $p_{ch}(k)$, whereas discharging power is shown by $p_{dch}(k)$ for the BESS at time k, respectively. Similarly, $x_{ch}(k)$ and $x_{dch}(k)$ are binary variables and denote the charging and discharging status of the BESS at time period k, respectively; $soc(k)$ is the status of charge of BESS at time k; Δk is the span of the time interval; v_b is the capability of the BESS; μ_{ch} and μ_{dch} are the competency of charging and discharging, respectively. State of charge decides the voltage level of the battery.

G. Stability Analysis of AVF

The study of the performance of the AVF can be completed through its transfer function. The stability analysis is an important part of any filter configuration and can be obtained from the bode plot stability study technique. The input/output relationship between load current and fundamental load current is shown by the transfer function. It is derived from the block diagram shown in Fig. 3(a) and represented as

$$H(S) = \frac{\omega k_f(s + \omega k_f + j\omega)}{(s+\omega k_f)^2 + \omega^2}. \tag{37}$$

From (37), bode plot is obtained. The value of ω is generally chosen to be 50 Hz because in most of the countries, it is adapted as a grid frequency. But other values can also be taken in proper range. A four number of plots are represented for four values of k_f (1, 0.73, 0.65, 0.85), which is known as design coefficient of AVF. As per four different values four transfer function g_1, g_2, g_3, and g_4 are calculated. From Fig. 3(b), it is evident that for any value of design coefficient, the phase and gain of AVF for the fundamental frequency signal is zero and for remaining frequencies, signals are either shifted or attenuated. From this, it can be concluded that AVF is accurately performing the extraction of desired component. Furthermore, it can be noticed that, decreasing the value of k_f, the filter becomes more selective. Though, the fractional multiple of k_f represents the number of cycles needed to rebuild the required frequency constituent. Thus, a compromise between selectivity and speediness should be taken into consideration, if the input signal comprises more harmonic constituent.

V. Results and Discussion

The performance of the generator has been studied under various operating conditions and results are presented in this section. The proposed control algorithm is implemented by using MATLAB/Simulink tool for controlled operation of VSC. This method uses the vectorial properties of the single-phase input signal in the $\alpha\beta$ orientation frame in order to obtain the diverse harmonic constituents. The important aspect of this algorithm is its ability to generate in phase and oscillating component along with frequency from the simple steps. Horizontal axis wind turbine is supplying mechanical power to the rotor of the generator. The VSC is designed and controlled for voltage control, frequency control, and mitigation of harmonics. Figs. 4–8 portray performance results and salient points discussed in subsequent sections.

A. Control Signal Generation or Performance of the AVF Control Algorithm

The harmonization method based AVF capability is evaluated by way of MATLAB/Simulink. The parameters of AVF are set as $k_f = 0.73$ and $\omega = 50$ initially. Fig. 4 shows the response of the AVF when the input signal (load current that is distorted) comprises fundamental and harmonics components is applied. The various control actions are performed using discrete operation of (20). The sampling frequency is 10 kHz, and the number of periods to restore the input signal is selected to be $k_f = 0.73$. Moreover at the moment ($t = 4.5$ s), k_f is changed to 0.85 and observed the output of the filter. It can be seen from the waveforms that input signal is recreated accurately as likely in both cases of k_f. However, the sampling frequency affects the construction process, therefore, it should be chosen carefully.

The initial condition for the integrator that gives estimated frequency is set as 100 π rad/s, or in other words, it is set as the

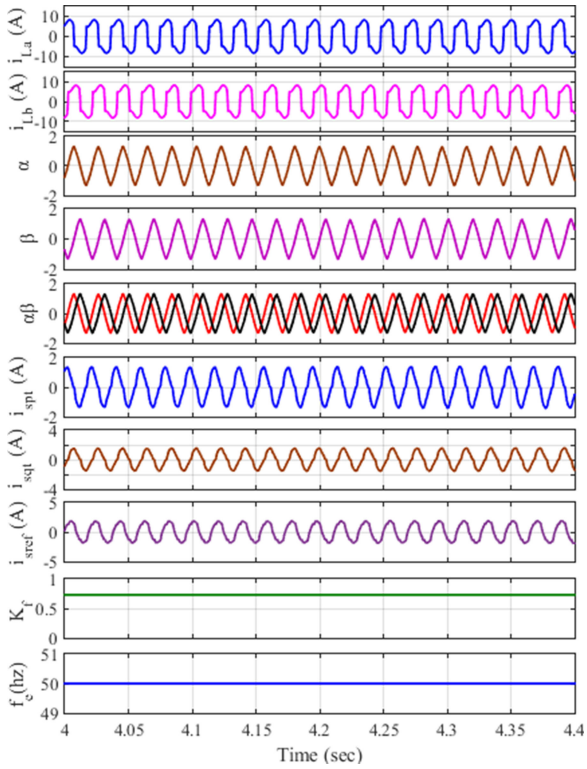

Fig. 4. Generated control signals by AVF.

nominal frequency (50 Hz). Fig. 4 depicts the various transitional signals of the AVF control algorithm that consists sensed load current (i_{La}) and its phase-shifted component (i_{Lb}) as input feedback. During the process of reference source current (i_s^*) generation, other intermediate signals such as fundamental components in vectorial form (i_α and i_β), reference active power component of source current (i_{spt}), amplitude of reference oscillating power component of source current (i_{sqt}), filter coefficient (k_f) and frequency (f) are also obtained.

B. Performance of the SEIG in the Fixed/Variable Wind Speed Mode Under Linear Load

The dynamic performance of an SEIG controlled by VSC, feeding linear load under fixed/variable wind speed mode is shown in Fig. 5(a) and (b). The parameters that are observed here are source voltage at PCC (v_s), source current (i_s), load current (i_L), compensator current (i_c), magnitude of terminal voltage (v_t), frequency (f), wind speed (v_w), rotor speed (w_r), battery voltage (v_b), and battery current(i_b). Under fixed wind velocity mode operation of the SEIG, wind velocity (v_w) is considered to be 12 m/s and all waveforms are harmonics free because of linear load ($i_L = 9.7$ A, 0.85 pf lag) connected to generator. In this mode, compensator is supplying ($i_c = 5.18$ A) reactive current demanded by generator and load, therefore, SEIG is supplying only real component of load current. The waveform of compensator current is also sinusoidal. For the said wind speed generator rotor is rotating at ($w_r = 168$ rad/s). Now for transient analysis, load is changed from the level ($i_L = 9.7$ A,0.85 pf) to level ($i_L = 11$ A, 0.75 pf) at time (t) equal to 4.2 s. Source current remains almost constant while current flowing in the battery decreases due to increased power flow into the load. In addition, voltage level of the battery remains fixed with some

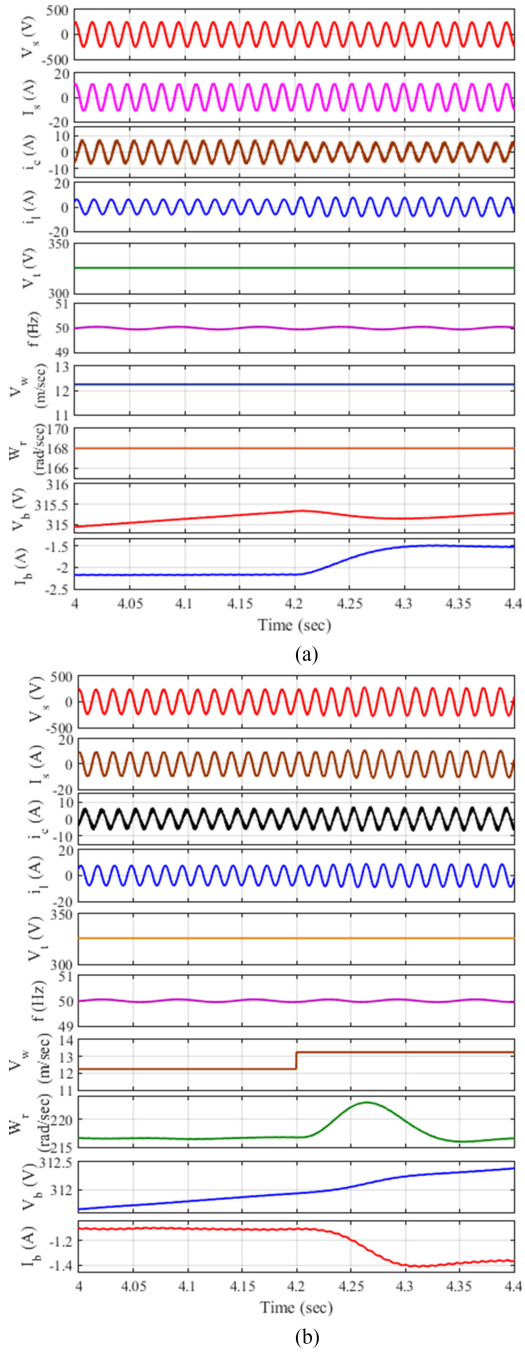

Fig. 5. (a) Performance of the SEIG under linear load with fixed speed. (b) Performance of the SEIG under linear load with variable speed.

fluctuations. In this case, dump control is inactive because of power flow toward battery is reducing, and toward load, it is increasing while generation is not increased. Hence, there is not excess power left for dumping. The other parameters such as frequency remains fixed around their reference value of 50 Hz. These are shown in Fig. 5(a). Now in variable wind velocity operation of the SEIG, velocity of wind (v_w) is changed to 13.5 m/s at time (t) equal to 4.2 s. At the instant, velocity of the rotor increases, frequency rise occurs simultaneously. Therefore, effective utilization factor of capacitor is reduced and hence capacity of excitation capacitor for supplying the reactive power needs to excite the generator is reduced. Apart from this, the value of mutual impedance and self-impedance of the SEIG

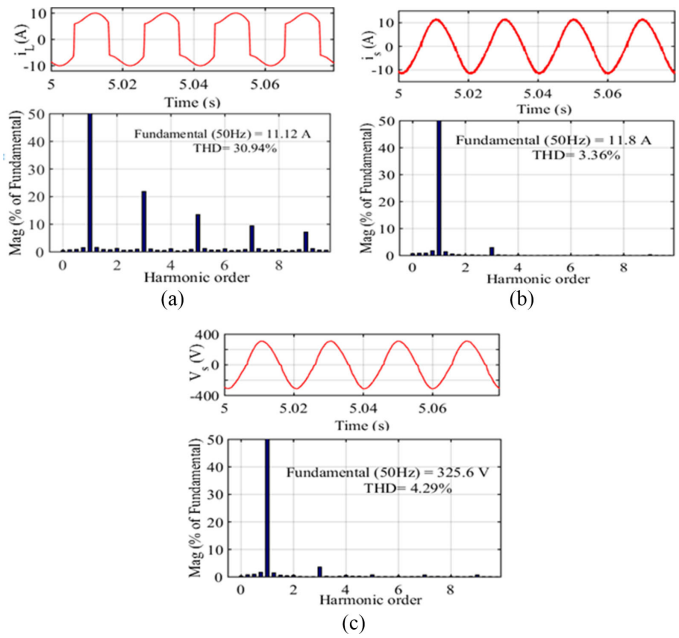

Fig. 6. Harmonic spectra: (a) Load current, (b) source current, and (c) source voltage, of the SEIG under fixed speed and nonlinear load.

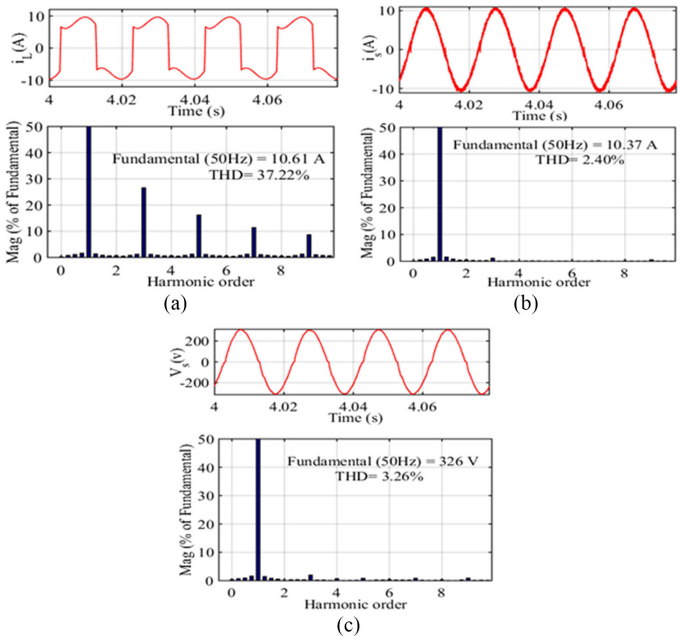

Fig. 7. Harmonic spectra; (a) Load current, (b) source current, and (c) source voltage, of the SEIG under variable speed and nonlinear load.

will rise. This results in more voltage drop across the PCC terminals. The AVF algorithms sensed the variation in voltage and frequency and generate the reference source current for control of VSC in such a way that it generates and injects more compensating current (means supplying more reactive power to generator) to mitigate the voltage variation. This effect can be seen from Fig. 5(b). Now with increased speed of the wind at time (*t*) equal to 4.2 s, turbine generates more torque ($T_l \alpha\, N^2$), hence, power generation will also increase. For maintaining the frequency around reference value, active power balance is needed at the terminal of the generator. Due to constant load considered here, with increased generation, battery charging level will increase terminal voltage. Source current level will rise for the same load demand and dump load will be turn on with the help of coordinated control to limit the battery current flow. Thus with this kind of power balance, frequency and terminal voltage will be maintained. These things will be taken care by AVF itself. Remaining parameters are as on the lines of fixed speed maintained at their reference value. The parameters are plotted in Fig. 5(b).

Total harmonic distortion (THD) of the load current, source current and source voltage under rated loading condition with fixed wind speed are found to be 30.94%, 3.36%, and 4.29%, respectively. The harmonic spectra along with fast Fourier transform (FFT) signal window is shown in Fig. 6(a)–(c). THD of the load current, source current, and source voltage under rated loading condition and variable wind speed are found to be 37.22%, 2.40%, and 3.26%, respectively. These values are well within limits of IEEE-519-2014 standards. The harmonic spectra along with FFT signal window are shown in Fig. 7(a)–(c).

C. Performance Evaluation of the SEIG in the Fixed/Variable Wind Speed Mode Under Nonlinear Load

The transient performance of an SEIG operated and controlled by VSC for the fixed/variable wind speed mode under nonlinear load is shown in Fig. 8(a) and (b). The single-phase diode bridge rectifier with *RL* load connected on dc side has been taken as nonlinear load. The loading condition is same as case B described above except the diode bridge. The observed parameters are source voltage at PCC (v_s), source current (i_s), load current (i_L), compensator current (i_c), magnitude of terminal voltage (v_t), source frequency (*f*), wind speed (v_w), rotor speed (w_r), battery voltage (v_b), and battery current (i_b). Under fixed wind velocity mode operation of the SEIG, wind velocity (v_w) is considered to be 12 m/s, the voltage amplitude at PCC is observed at 320 V and source current is ($i_s = 8.2$ A) for ($i_L = 10.6$ A, 0.8 pf) connected load. In this condition, reactive and harmonics component of load current is supplied by VSC ($i_c = 7.8$ A) in Fig. 8(a), and hence, SEIG is supplying only real fundamental component of load current. Due to nonlinear loading on the generator, a harmonic component along with reactive component has to be compensated by VSC, hence, the value of compensating current in this case is more than the linear load. For the said wind speed generator's rotor is rotating at ($w_r = 168$ rad/ s). The other parameters such as frequency remains fixed at their reference value of 50 Hz. These are shown in Fig. 8(a). Battery dynamics is similar to CASE B under load variation. Now, in variable wind velocity mode operation of the SEIG velocity of wind (v_w) is changed to 13 m/s at time (*t*) equal to 4.2 s. Due to presence of nonlinearity in the nature of load, source current nature will be no longer sinusoidal. This effect will be reflected on the machine parameters because it is running in standalone mode. Again on the similar lines as case B, the AVF will sense the PCC voltage, source current and load current and generate the reference source current for gate pulse generation to control the VSC. The VSC injects compensating current at PCC, which cancels the harmonics from the source current. In addition to it, reactive component of load current is also compensated and hence source current remains sinusoidal and its value would be the real component of load current. This effect can be seen from Fig. 8(b). Now with increased speed of the wind, turbine generates more torque ($T_e \alpha\, \mathrm{N}^2$), hence, power generation will also

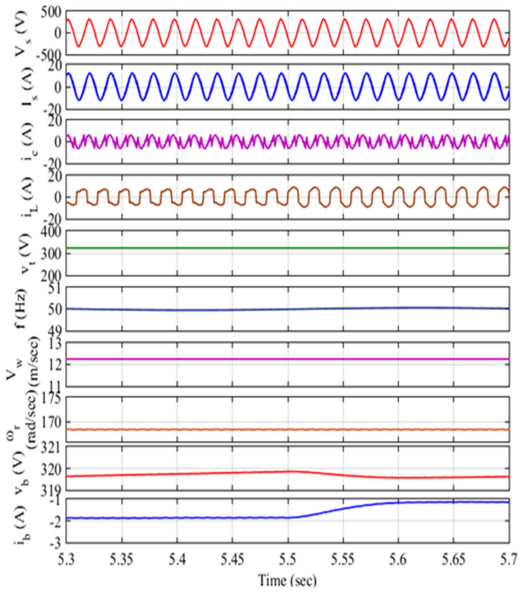

(a)

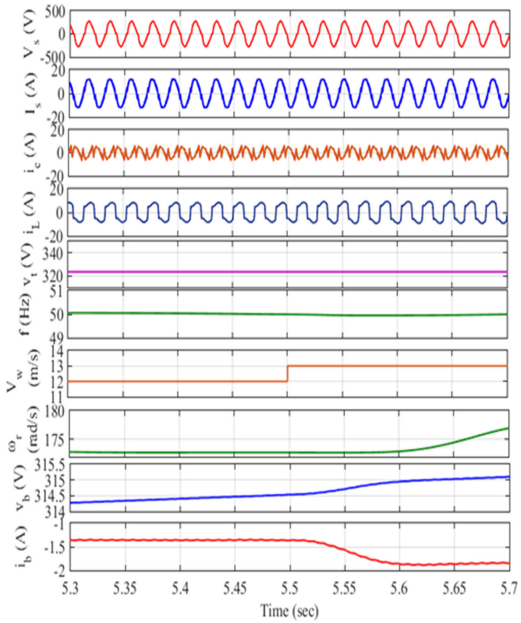

(b)

Fig. 8. (a) Performance of the SEIG under nonlinear load with fixed speed. (b) Performance of the SEIG under nonlinear load with variable speed.

increase. For maintaining the frequency around reference value, active power balance is needed at the terminal of the generator. Due to constant terminal voltage, source current level will rise for the same load demand and one coordinated dump controller is switched on for maintaining the frequency and charging rate of battery.

D. Power Flow Control of Battery and Dump Load

The active power exchange from/to the battery and to the dump load is shown in Fig. 9. Here, from the simulation results, it is clear that as per the load variation battery charges or discharges to control the frequency in coordination with dump load. The dump controller interferes only when battery is near to attain its optimum voltage level. In Fig. 9, at ($t = 4$ to 5 s) there is no

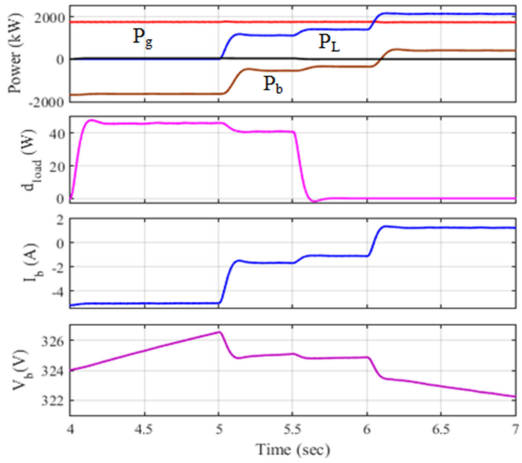

Fig. 9. Dynamics of BESS with variation in load and dump controller.

load connected from the generator and all the generated power is stored in the battery. Voltage of battery reaches its optimum value of 325 V. Therefore, a coordinated dump controller is turned on to divert some generated power to the dump load.

At t = 6 s, generator is overloaded, therefore, to maintain the frequency, battery started discharging, due to which voltage of battery will be going down and battery current reverses its direction.

VI. Experimental Validation

The sample model of the proposed system using the AVF-based control technique has been developed in its prototype form, analyzed, and tested in laboratory environment in real time on FPGAXC3S5000 controller under a nonlinear loading conditions. This controller comprises 3.3-GHz processor core with core activation level up to 8. Moreover, this runs on red hat Linux operating system. There are 32 channels of analog input/output and 32 channel of digital input/output are provided in it. The voltage level capacity of ADC/DAC is 16 V. The results are taken under steady-state and dynamical conditions of the load. Outstanding frequency and voltage control, in addition with harmonic alleviation capability of the AVF is seen in the observed test results shown in Figs. 10–11. The sampling frequency of 50 kHz is considered to generate C-code in FPGA during real-time testing of the system. The FPGA is used for the real-time implementation of the proposed AVF algorithm for reference source current computation and gating signal generation. Dynamic performance of control algorithms and generator is discussed as follows.

A. Voltage and Frequency Control of the SEIG With Different Control Signal Generation

The AVF control algorithm is implemented in real time on FPGAXC3S5000 and results are shown in Fig. 10(a)–(f). In Fig. 10(a), source voltage (v_s), source current (i_s), and compensator current (i_c) under variable load current (i_L) is shown. It is clear from the results, supply voltage and current are fully controlled under different loading conditions. In Fig. 10(b), load is injected from no load condition at some time and waveforms source voltage, source current and compensating current is observed. In this case, remarkable change in compensator current

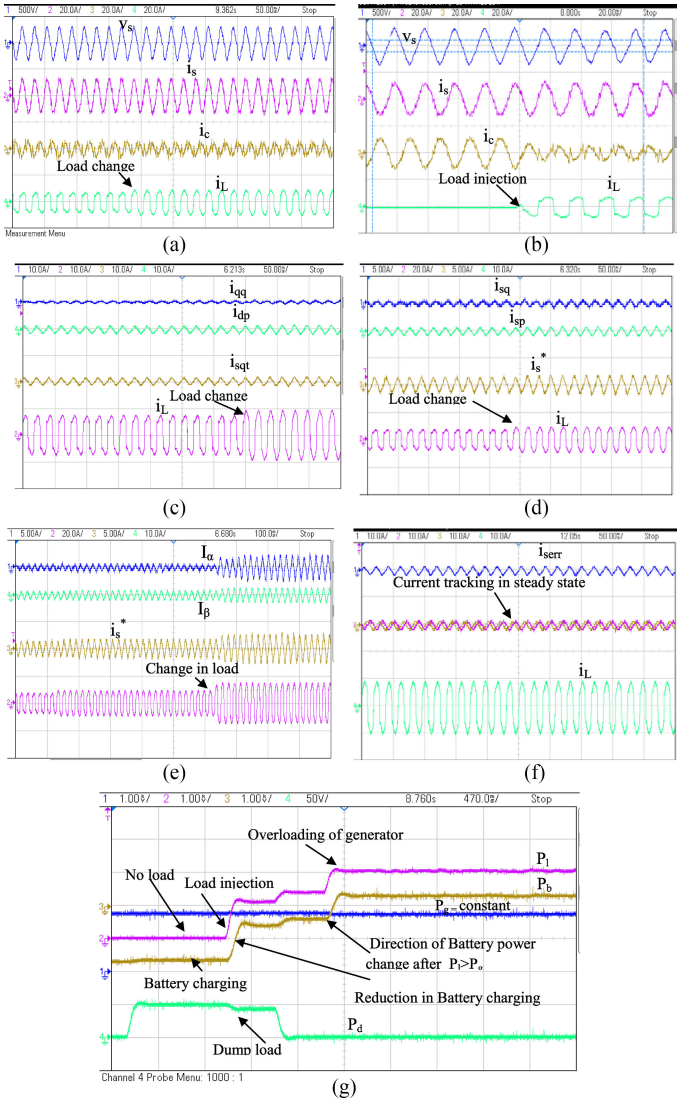

Fig. 10. Dynamic performance of the system with BESS under nonlinear load variation. (a) Test results of V_s, i_s, i_c, and i_L when load is changed at some time (Channel 1 is 500 V/div, channel 2: 20 A/div, channel 3: 20 A/div, channel 4: 20 A/div). (b) Test results of V_s, i_s, i_c, i_L when load is injected from no load (Channel 1 is 500 V/div, channel 2: 20 A/div, channel 3: 20 A/div, channel 4: 20 A/div). (c) Test results of control parameter i_{qq}, i_{dp}, i_{sqt} under load current variation I_L (Channel 1 is 10 A/div, channel 2: 10 A/div, channel 3: 10 A/div, channel 4: 10 A/div). (d) Test results of control parameter i_{sqt}, i_{spt}, i_s^* under load current variation I_L (Channel 1 is 5 A/div, channel 2: 20 A/div, channel 3: 5 A/div, channel 4:10 V/div). (e) Test result of vectorial component of load i_α, i_β, and reference source current i_s* current with change in load current (Channel 1 is 5 A/div, channel 2: 20 A/div, channel 3: 5 A/div, channel 4: 10 A/div). (f) Waveform of $i_{\rm serr}$ and current tracking under steady state (Channel 1 is 10 A/div, channel 2: 10 A/div, channel 3: 10 A/div, channel 4: 10 A/div). (g) Power exchange among the SEIG (P_g), load (P_l), battery-based controller (P_b) and dump load (P_d) under different dynamical conditions (Channel 1 is 1 kV/div, channel 2: 1 kV/div, channel 3: 1 kV/div, channel 4: 50 V/div).

has been seen due to change in battery charging current. When generator is running at no load, generated power is going to be stored in the BESS while on application of load on generator terminal, charging of the battery weakens therefore battery current that is flowing through compensator reduces when load is increased. From Fig. 10(c)–(e), different intermediate control signals mentioned in the following captions are depicted.

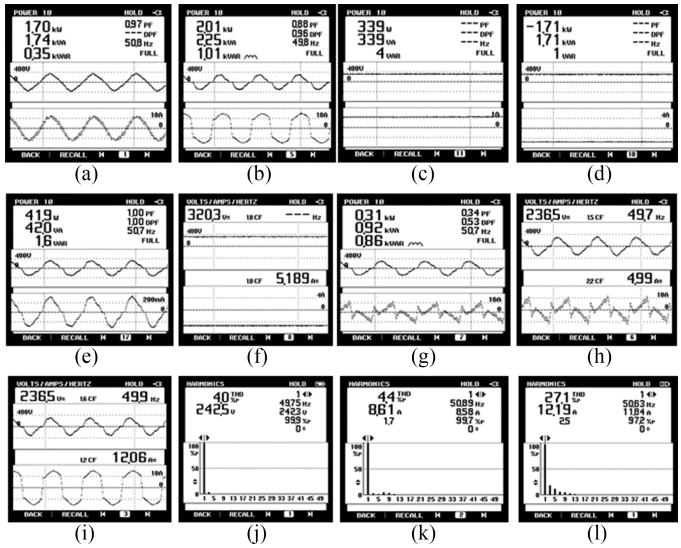

Fig. 11. Experimental results showing performance of the SEIG-VSC system. (a) Generator power, (b) load power, and (c) battery power in discharging mode when generator is overloaded. (d) Battery power during charging (when generator is at no load). (e) Dump load power to limit the battery charging. (f) Battery voltage level during discharging, (g) power of compensator, (h) waveform and rms value of compensator current and voltage, and (i) waveform and rms value of load current and voltage at PCC. (j) Harmonic spectrum showing THD in source voltage. (k) Harmonic spectrum showing THD in source current. (l) Harmonic spectrum showing THD in load current.

B. Dynamic Performance of the SEIG-STATCOM With BESS Under Nonlinear Load

The dynamic performance and power flow under various operating conditions of generator has been discussed in following cases.

Case (1): When generator is running under no load (i.e., $P_l = 0$).

When generator is being running under no load, generated power is either stored in BESS or dumped into dump load or dumped the excess generated power beyond the storage capacity for control of voltage and frequency. Here, in this paper, authors have tried to implement the coordinated control of BESS and dump load so that battery should not be overcharged (i.e., beyond its normal capacity), and hence, excess power would be dumped into dump load for betterment of the battery life. In the experimentation, 1.7 kW, 1.74 kVA, 0.35 kvar, 0.97 pf of power is generated. At beginning, when generator is not connected to the load, this whole amount of power is stored in the battery as per its charging level. After optimal level of charging, dump load is connected and a portion of this power is diverted into it to protect the life of the battery. This is shown in Fig. 10(g).

Case (2): When generator is loaded below its generation level ($0 < P_l < P_g$).

From Fig. 10(g), it is clear from the middle part of the graph that generator loading under below generation level, battery charging current reduces, i.e., power flow toward battery is also reduces. Generator is supplying power to the load and difference power between generator and load is flowing into the battery. Steady-state performance is shown in Fig. 11(a)–(i), for this case, where 339 W is flowing as a difference power into the battery.

TABLE II
PERFORMANCE OF VSC IN TERMS OF POWER QUALITY

Sr. No.	Mode of operation	Power quality indices						
		v_s	i_s	i_L	i_c	% THD in v_s	% THD in i_s	% THD in i_L
1.	$(P_L = 0)$	236 V	10.07 A	0 A	10.07 A	3.7%	4.1%	–
2.	$(0 < P_l < P_g)$	236.5 V	10.07 A	8.6 A	5.6 A	4.0%	4.4%	27.9%
3.	When $(P_l > P_g)$	236.5 V	10.5 A	12.19 A	7.07 A (reverse)	4.04%	4.1%	27.1%

TABLE III
PERFORMANCE OF VSC IN TERMS OF POWER BALANCE

Sr. No.	Mode of operation	Performance of VSC for power balance						
		P_g	P_L	P_c	V_b	i_b	P_d	Remarks
1.	$P_L = 0$	1.7 kW	0 kW	1.7 kW	320 V	5.1 A	42 W	P_d is on due to optimal control of BESS
2.	$(0 < P_l < P_g)$	1.7 kW	1.4 kW	339 W	320 V	3.4 A	–	–
3.	$(P_l > P_g)$	1.7 kW	2.01 kW	320 W	320 V	3.1 A	–	–

Case (3): When generator is loaded above its generation level $(P_l > P_g)$.

When generator is running with overloaded condition, BESS is supplying power to the load for frequency control. From Fig. 10(g), it is evident that AVF control is able to change the direction of power flow in the battery. During no-load or light-load conditions, battery had stored the energy that is used for overloading or peak time. Again the steady-state operations of whole system are depicted here in Fig. 11(a)–(i). In addition to frequency and voltage control, AVF is also maintaining the power quality features of the SEIG. From Fig. 11(j)–(l), power quality indices are presented in terms of THD. Nonlinear load current is creating 27% THD while supply current and source voltage contains around 4% (below 5% level as per IEEE-519-2014 Standard) after applying AVF control. Detail results of the SEIG performance of power quality and power balance are tabulated in Tables II and III, respectively.

VII. CONCLUSION

Voltage and frequency control of the SEIG along with power quality features is a significant issue in standalone mode of operation driven by wind turbines. Due to variable nature of wind velocity, it affects the working of the SEIG and current control strategy used to handle the VSC. This paper presents a control approach utilizing the vectorial adaptive filters. The projected method allows us to guess the grid frequency and the various harmonic frequency constituents. The steps for designing the methodology has been offered in this paper and a vital issue such as the selection of the filter coefficient has been presented with the help of transfer function approach in order to attain a needed performance of the system. The algorithm has been tested with simulation followed by experimental validation found satisfactory. In addition to it, generator performance and design are also validated through the FEM software.

APPENDIX A

A1. Rating and parameters of the single-phase SEIG

Ratings: 2.2 kW, 220 V, 50 Hz, and 4-pole; Parameters: Main winding stator: $R_{\rm ms} = 2.93\,\Omega$, $L_{\rm ms} = 0.0267544\,$H, main winding rotor: $R_{\rm mr} = 3.3077\,\Omega$, $L_{\rm mr} = 0.017544\,$H, main winding mutual inductance: $L_{\rm ms} = 0.13814\,$H, auxiliary winding stator: $R_{\rm as} = 5.0268\,\Omega$, $L_{\rm as} = 0.024007$ H; inertia $= 0.00290763\,\text{J}\,(\text{kg}\cdot\text{m}^2)$, pole pair $= 2$, auxiliary to main winding turns ratio $= 1.25$; excitation capacitor $= 80\,\mu$F;

A2. Compensator Parameters

$Ls = 4\,$mH; $R_f = 8\,\Omega$; $C_f = 12\,\mu$F; $C_{dc} = 8000\,\mu$F.

A3. BESS Parameters

Lithium-ion type, 400 V, 150 A·H, SOC (10% to 90%), $r_s = 0.05\,\Omega$.

Dump load: 240 V, 100 Ω, 500 W.

APPENDIX B

B1. DC-bus voltage

The needed dc-bus voltage of VSC must be more than twice the peak of the phase voltage at the ac terminals of VSC [14]. The dc-bus voltage is computed as

$$V_{dc} = \frac{2^*\sqrt{2}V_L}{m^*\sqrt{3}}. \tag{B.1}$$

Here, *m* is designated as the modulation factor; taken 1 for this case, and V_L is taken as the rms value of line voltage. Therefore, V_{dc} is calculated with equation (B_1) and obtained as 376 V for V_L (230 V) and it has been chosen as 400 V.

B2. Selection of Battery

The battery is an energy storage unit, its energy is represented in kilowatthour (kWh) [11]. The size of battery for wind energy conversion system (WECS) is decided based on wind speed profile at the site and nature of load connected at WECS. Large storage capacity may facilitate better contingency handling, but increase the initial investment and maintenance problems. Therefore, a compromise has been made in deciding the size of battery storage unit. Further, as the required V_{dc} is more than 376 V, therefore, the minimum battery rack voltage should be 400 V. A battery rack with capacity of 2.8 kWh is used for

the energy storage in this prototype. For the dc-bus voltage of 400 V, 36 units of 12 V, 7 Ah are connected in series.

B3. AC Inductor

The design of an interfacing inductor depends on allowable ripple in the current (i_{crp}), the voltage at the dc bus (V_{dc}) and switching frequency (f_s) of VSC and is given as [14]

$$L_i = \frac{\sqrt{3} m V_{dc}}{12 p f_s i_{crp}} \tag{B.2}$$

where m is the modulation index and p is the overloading factor. Considering $m = 1$, $V_{dc} = 400\,\text{V}$, $p = 1.2$, $i_{crp} = 1.5\%$ and $fs = 10\,\text{kHz}$, the value of L_i is obtained as 3.2 mH. A round off value of 4 mH is selected in this exploration.

REFERENCES

[1] J. M. Chapallaz, J. D. Ghali, P. Eichenberger, and G. Fischer, *Manual on Induction Motors used as Generators*. Berlin, Germany: Springer, 1992.

[2] L. L. Lai and T. F. Chan, *Distributed Generation: Induction and Permanent Magnet Generators*. Hoboken, NJ, USA: Wiley, 2007.

[3] M. Stiebler, *Wind Energy Systems for Electric Power Generation (Green Energy and Technology)*. Berlin, Germany: Springer-Verlag, 2008.

[4] S. S. Murthy, B. Singh, and V. Sandeep, "A novel and comprehensive performance analysis of a single-phase two-winding self-excited induction generator," *IEEE Trans. Energy Convers.*, vol. 27, no. 1, pp. 117–127, Mar. 2012.

[5] F. Blaabjerg, R. Teodorescu, M. Liserre, and A. Timbus, "Overview of control and grid synchronization for distributed power generation systems," *IEEE Trans. Ind. Electron.*, vol. 53, no. 5, pp. 1398–1409, Oct. 2006.

[6] B. Singh, G. Kasal, A. Charndra, and K.-A. Haddad, "Battery based voltage and frequency controller for parallel operated isolated asynchronous generators," in *Proc. IEEE Int. Symp. Ind. Electron.*, Vigo, Spain, Jun. 4–7, 2007, pp. 883–888.

[7] V. Rajagopal, B. Singh, and G. K. Kasal, "Electronic load controller with power quality improvement of isolated induction generator for small hydro power generation," *IET Renewable Power Gener.*, vol. 5, no. 2, pp. 202–213, 2011.

[8] U. K. Rao, M. K. Mishra, and A. Ghosh, "Control strategies for load compensation using instantaneous symmetrical component theory under different supply voltages," *IEEE Trans. Power Del.*, vol. 23, no. 4, pp. 2310–2317, Oct. 2008.

[9] S. Huang and J. Wu, "A control algorithm for three-phase three wired active power filters under non-ideal mains voltage," *IEEE Trans. Power Electron.*, vol. 14, no. 4, pp. 753–760, Jul. 1999.

[10] L. M. Tolbert and T. G. Habler, "Comparison of time-based non-active power definitions for active filtering," in *Proc. IEEE Int. Power Electron. Congr. Tech. Proc.*, Acapulco, Mexico, 2000, pp. 73–79.

[11] V. Cardenas, L. Moran, A. Bahamondes, and J. Dixon, "Comparative study of real time reference generation techniques for four-wire shunt active power filters," in *Proc. IEEE 34th Annu. Power Electron. Spec. Conf.*, Acapulco, Mexico, 2003, pp. 791–796.

[12] M. Karimi-Ghartemani, H. Karimi, and A. Bakhshai, "A filtering technique for three-phase power systems," *IEEE Trans. Instrum. Meas.*, vol. 58, no. 2, pp. 389–396, Feb. 2009.

[13] B. Singh, S. S. Murthy, and S. Gupta, "A voltage and frequency controller for self-excited induction generators," *J. Elect. Power Compon. Syst.*, vol. 34, pp. 141–157, 2006.

[14] S. R. Arya and B. Singh, "Performance of DSTATCOM using leaky LMS control algorithm," *IEEE J. Emerg. Sel. Topics Power Electron.*, vol. 1, no. 2, pp. 104–113, Jun. 2013.

[15] S. Shinnaka, "A robust single-phase PLL system with stable and fast tracking," *IEEE Trans. Ind. Appl.*, vol. 44, no. 2, pp. 624–633, Mar./Apr. 2008.

[16] X. Guo, W. Wu, and Z. Chen, "Multiple-complex coefficient-filter-based phase-locked loop and synchronization technique for three-phase grid interfaced converters in distributed utility networks," *IEEE Trans. Ind. Electron.*, vol. 58, no. 4, pp. 1194–1204, Apr. 2011.

[17] R. Arablouei, S. Werner, and K. Dogançay, "Analysis of the gradient-descent total least-squares adaptive filtering algorithm," *IEEE Trans. Signal Process.*, vol. 62, no. 5, pp. 1256–1264, Mar. 2014.

[18] Z. Shuai, A. Luo, C. Tu, and D. Liu, "New control method of injection type hybrid active power filter," *IET Power Electron.*, vol. 4, no. 9, pp. 1051–1057, 2011.

[19] A. Bhattacharya, C. Chakraborty, and S. Bhattacharya, "Shunt compensation," *IEEE Trans. Ind. Electron. Mag.*, vol. 3, no. 3, pp. 38–49, Sep. 2009.

[20] Y. Suresh, A. K. Panda, and M. Suresh, "Real-time implementation of adaptive fuzzy hysteresis-band current control technique for shunt active power filters," *IET Power Electron.*, vol. 5, no. 7, pp. 1188–1195, 2012.

[21] J.-C. Wu, H.-L. Jou, Y.-T. Feng, W.-P. Hsu, M.-S. Huang, and W.-J. Hou, "Novel circuit topology for three-phase active power filter," *IEEE Trans. Power Del.*, vol. 22, no. 1, pp. 444–449, Jan. 2007.

[22] D. A. Bristow, M. Tharayil, and A. G. Alleynea, "Learning-based method for high-performance tracking control," *IEEE Control Syst. Mag.*, vol. 26, no. 3, pp. 96–114, Jun. 2006.

[23] T. F. Chan, L. L. Lai, and L.-T. Yan, "Finite element analysis of a single-phase grid-connected induction generator with the Steinmetz connection," *IEEE Trans. Energy Convers.*, vol. 18, no. 2, pp. 321–329, Jun. 2003.

[24] X. Wang, L. Sun, F. Wen, M. A. Salam, and S. P. Ang, "Control strategies of battery energy storage systems for smoothing wind power fluctuations," Project Report from National Natural Science Foundation of China (51477151), and a project from State Grid Zhejiang Electric Power Corporation (5211DS14000X), 2013.

[25] J. Fei and J. Zhou, "Robust adaptive control of MEMS triaxial gyroscope using fuzzy compensator," *IEEE Trans. Syst., Man, Cybern. B, Cybern.*, vol. 42, no. 6, pp. 1599–1607, Dec. 2012.

[26] J. Fei and C. Lu, "Adaptive sliding mode control of dynamic systems using double loop recurrent neural network structure," *IEEE Trans. Neural Netw. Learn. Syst.*, vol. PP, no. 99, pp. 1–12, doi: 10.1109/TNNLS.2017.2672998.

[27] J. Fei and H. Ding, "Adaptive sliding mode control of dynamic system using RBF neural network," *J. Nonlinear Dyn.*, vol. 70, no. 2, pp. 1563–1573, 2012.

[28] J. Fei and M. Xin, "An adaptive fuzzy sliding mode controller for MEMS triaxial gyroscope with angular velocity estimation," *J. Springer*, vol. 70, no. 1, pp. 97–109, Oct. 2012.

[29] S. Vazquez, J. A. Sanchez, M. R. Reyes, J. I. Leon, and J. M. Carrasco, "Adaptive vectorial filter for grid synchronization of power converters under unbalanced and/or distorted grid conditions," *IEEE Trans. Ind. Electron.*, vol. 61, no. 3, pp. 1355–1367, Mar. 2014.

Ashutosh K. Giri received his Bachelor of Engineering in electrical engineering from the College of Technology, G. B. Pant University of Agriculture and Technology, Pantnagar Uttarakhand, India, in 2002, and the M. Tech. in electrical engineering with specialization in Power System from the L.D. College of Engineering, Ahmedabad, Gujarat, India, in 2005. He is currently at the Department of Electrical Engineering, Sardar Vallabh National Institute of Technology, Surat India, where he is working toward Ph.D. degree under Quality Improvement Program.

In May 2011, he joined Department of Electrical Engineering, Government Engineering College, Bharuch, as an Assistant Professor. His fields of interest include power quality and power electronics application in distributed power generation.

Amin Qureshi received the Bachelor of Engineering degree in electrical engineering from L.E. College Morbi, Gujarat, India, in 2014, and the M.Tech. degree in electrical engineering with specialization in power electronics and electrical drives from the Sardar Vallabhbhai National Institute of Technology, Surat, India, in 2017.

He was associated with Innovative Telecom and Software Pvt., Ltd., Surat, from 2014 to 2015. His research interests include power electronics and distributed power generation.

Sabha Raj Arya (M'12–SM'15) received Bachelor of Engineering (electrical engineering) degree from Government Engineering College Jabalpur, in 2002, the Master of Technology (power electronics) degree from Motilal National Institute of Technology, Allahabad, in 2004, and Ph.D. degree in electrical engineering from the Indian Institute of Technology (I.I.T) Delhi, New Delhi, India, in 2014. He is joined as Assistant Professor, Department of Electrical Engineering, Sardar Vallabhbhai National Institute of Technology, Surat. His fields of interest include power quality, design of power filters, and distributed power generation.

He received Two National Awards namely INAE Young Engineer Award from Indian National Academy of Engineering, POSOCO Power System Award from Power Grid Corporation of India in the year of 2014 for his research work. He also received Amit Garg Memorial Research Award-2014 from I.I.T Delhi from the high impact publication in a quality journal during the session 2013–2014

Rakesh Maurya (M'17) received B.Tech degree in electrical engineering from the Kamla Nehru Institute of Technology Sultanpur, Uttar Pradesh, in 1998, and the M.Tech (degree in power electronics and electric drive, and the Ph.D degree in electrical engineering from the Indian Institute of Technology Roorkee, India, in 2002 and 2014, respectively.

Currently, he is serving as faculty member in the Department of Electrical Engineering, Sardar Vallabhbhai National Institute of Technology Surat, Gujarat, India. His fields of interest include design of switching power converters, high power factor AC/DC converters, advanced electric drives, and applications of real time simulator for the control of power converters.

Dr. Maurya is a Life Member of System Society of India.

B. Chitti Babu (SM'15) received the Ph.D. in electrical engineering from National Institute of Technology Rourkela, India in 2012.

He was with National Institute of Technology Rourkela, India as an Assistant Professor in Electrical Engineering from 2007 to 2013. He had two postdoctoral research appointments with Wroclaw University of Science & Technology, Poland, from Dec 2013–June 2014 and VSB-Technical University of Ostrava, Czech Republic from 2014 to 2015 and both the appointments have been sponsored by European Commission, U.K. In September 2016, he was appointed as an Assistant Professor in the Department of Electrical and Electronics Engineering, The University of Nottingham Malaysia Campus, Malaysia. His research interests include power electronics applications in smart distribution grid containing renewable energy sources and low-power electronics design, including photovoltaic energy systems.